Sensors and Actuators A 203 (2013) 149–153

Contents lists available at ScienceDirect

Sensors and Actuators A: Physical

journal homepage: www.elsevier.com/locate/sna

Analysis of a concentric coplanar capacitor for epidermal hydration sensing

Huanyu Cheng[a], Yihui Zhang[a,b], Xian Huang[c], John A. Rogers[c], Yonggang Huang[a,*]

[a] Departments of Mechanical Engineering and Civil and Environmental Engineering, Center for Engineering and Health, and Skin Disease Research Center, Northwestern University, Evanston, IL 60208, USA
[b] Center for Mechanics and Materials, Tsinghua University, Beijing 100084, China
[c] Department of Materials Science and Engineering, University of Illinois, Urbana, IL 61801, USA

ARTICLE INFO

Article history:
Received 10 July 2013
Received in revised form 20 August 2013
Accepted 23 August 2013
Available online 6 September 2013

Keywords:
Analytic expression impedance
Concentric coplanar capacitor
Epidermal hydration sensing
Single- and double-layer capacitors

ABSTRACT

Without conformal contact between hydration sensors and skin, measured signals (either capacitance or impedance) can be susceptible to artifacts associated with motion-induced changes and irreproducibility in contact. Devices with mechanical properties matched to the skin enable conformal contact and adhesion via the action of van der Waals forces alone, thereby facilitating accurate, reproducible measurements. Theoretical investigations of concentric coplanar capacitors in this type of 'epidermal' format yield analytic expressions of the impedance for single- and double-layer capacitors. The calculated dependence of impedance on material and geometric parameters agree well with finite element analysis and experiments, thereby providing important insights into the design of epidermal systems for hydration sensing.

Published by Elsevier B.V.

1. Introduction

Hydration levels in the skin are important because they correlate strongly to physiological status, various disease states and physical appearance [1,2]. Accurate measurement of hydration is, therefore, valuable in areas ranging from dermatology to cosmetology [3,4]. Typical approaches rely on electrical impedance, thermal conductivity or mechanical characteristics [5,6]. Among these parameters, impedance often provides the most direct indication because of the strong dependence of the conductivity and permittivity of the skin on its water content [7–9]. Options in simple and minimally invasive operation represent additional advantages of impedance measurements over others. Although commercially available tools exist for single point evaluation and multipoint mapping, the precision in real-world use can be limited by the inability of hard electrodes in such sensors to conform to the soft, curved textures of the skin.

The epidermal hydration sensing technology recently developed by Huang et al. [10] offers an alternative class of hydration sensing technology. The mechanical properties of these thin, stretchable devices are matched to the epidermis, to provide conformal contact driven by van der Waals interactions, in a way that is mechanically 'invisible' to the user. Differential impedance measurements in multiplexed arrays using this type of approach enable spatial mapping across relatively large areas. These attributes suggest potential for broad utility in personal healthcare.

This paper provides an analytical model to determine the capacitance and impedance in terms of the material and geometric parameters. There exist several studies on capacitance-based sensors, focusing on a variety of sensor geometries, including arc electrode [11], coplanar capacitor with two adjacent electrodes [12] and multiple coupled concentric electrodes [13]. Numerical analyses also exist for concentric coplanar capacitors [14,15]. Here, we introduce simple closed-form solutions for the concentric coplanar capacitors with single- and double-layer layouts. The analytical results are validated by the finite element method and experiments. The models not only offer important insights into the underlying physics, but they also establish useful guidance for device design and use. First, we introduce a model to study the types of concentric coplanar capacitors that have been explored in experiments [10], using a single-layered medium in Section 2. To account for the influence from both the stratum corneum and deep tissue layer, a double-layered model is developed in Section 3.

2. Concentric coplanar capacitor on a single-layered medium

An optical micrograph of an epidermal hydration sensing system is shown in Fig. 1(a). Impedance measured by this system, can also be derived from the electric field in the skin. The electric

* Corresponding author. Tel.: +1 847 467 3165.
E-mail address: y-huang@northwestern.edu (Y. Huang).

0924-4247/$ – see front matter. Published by Elsevier B.V.
http://dx.doi.org/10.1016/j.sna.2013.08.037

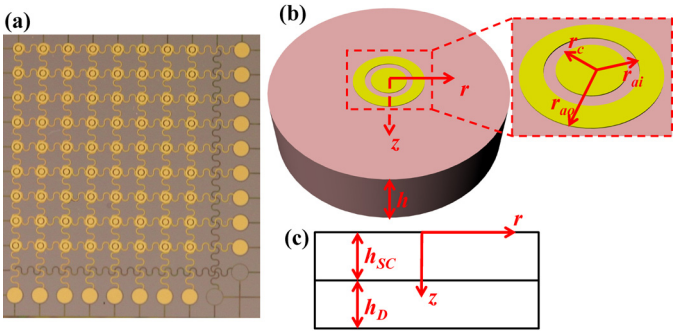

Fig. 1. (a) Optical micrograph of an epidermal hydration sensing system. (b) Schematic illustration of a concentric coplanar capacitor from 3-D perspective view of the single-layered model (inset: geometric parameters of concentric electrodes). (c) Cross-sectional view of double-layered model.

Fig. 1(a) is reprinted with permission from Ref. [10], Copyright 2013, IEEE Transactions on Biomedical Engineering.

potential φ satisfies Laplace's equation $\nabla^2\varphi = 0$ [16], where ∇^2 is the Laplace operator. Setting the coordinate origin at the center of the concentric electrodes, the Laplace's equation is given as:

$$\frac{\partial^2\varphi}{\partial r^2} + \frac{1}{r}\frac{\partial\varphi}{\partial r} + \frac{\partial^2\varphi}{\partial z^2} = 0, \tag{1}$$

where r is the radial distance from the central axis of electrodes and z is the depth from the electrode-skin interface as shown in Fig. 1(b). The potential difference between the inner circular (radius of r_c) and outer annulus (r_{ai} and r_{ao} for the inner and outer radii) electrodes is ΔV at the electrode-skin interface:

$$\varphi\big|_{z=0,0<r<r_c} - \varphi\big|_{z=0,r_{ai}<r<r_{ao}} = \Delta V. \tag{2}$$

The electric field intensity is the gradient of the electric potential $\vec{E}(r,z) = -\nabla\varphi(r,z)$ [16]. In the places without electrodes at this interface and at the bottom surface of the skin $z = h$, the normal component (in the z-direction) of the electric field intensity is zero [16]:

$$\left.\frac{\partial\varphi}{\partial z}\right|_{z=0,r_c<r<r_{ai}} = \left.\frac{\partial\varphi}{\partial z}\right|_{z=0,r_{ao}<r<\infty} = 0, \tag{3}$$

$$\left.\frac{\partial\varphi}{\partial z}\right|_{z=h} = 0. \tag{4}$$

Eqs. (1)–(4) are the Laplace equation with mixed boundary conditions, i.e., the Dirichlet boundary condition in Eq. (2) and Neumann boundary conditions in Eqs. (3)–(4). An approximate solution is obtained by replacing Eq. (2) with the Neumann boundary condition in terms of the charge Q in the following, where Q is to be determined in term of ΔV. The electric displacement $\vec{D}$ is given by $\vec{D} = \varepsilon\vec{E}$ [16], which ε is the permittivity of the medium layer. At the electrode–skin interface, the charge density $q(r) = D_m - D_{air}$, where $D_m = \vec{D}\big|_{z=0}\cdot\vec{n}$ and $D_{air} = 0$ are normal components of the electric displacements in the medium and air, respectively [16], and $\vec{n}$ is the unit normal at $z = 0$. The charge in the inner circular electrode, $Q = 2\pi\int_0^{r_c} q(r)\,r\,dr$, is then obtained as $Q = -2\pi\varepsilon\int_0^{r_c}\partial\varphi/\partial z\big|_{z=0} r\,dr$, which can be approximately expressed as:

$$-\left.\frac{\partial\varphi}{\partial z}\right|_{z=0,0<r<r_c} \approx \frac{Q}{\pi\varepsilon r_c^2} \tag{5}$$

by assuming a constant $\partial\varphi/\partial z\big|_{z=0}$ over the inner circular of electrode. The conservation of charge requires that the charge in the outer annulus electrode be $-Q$, which gives $-Q = -2\pi\varepsilon\int_{r_{ai}}^{r_{ao}}\partial\varphi/\partial z\big|_{z=0} r\,dr$, or approximately:

$$-\left.\frac{\partial\varphi}{\partial z}\right|_{z=0,r_{ai}<r<r_{ao}} \approx -\frac{Q}{\pi\varepsilon\left(r_{ao}^2 - r_{ai}^2\right)} \tag{6}$$

by assuming another constant $\partial\varphi/\partial z\big|_{z=0}$ over the outer annulus electrode. The approximation changes the Dirichlet boundary condition in Eq. (2) to Neumann boundary conditions in Eqs. (5) and (6), leading to a Laplace equation with all Neumann boundary conditions. The problem now becomes rather easier to solve than the previous equation with mixed boundary conditions. The electric potential φ, obtained from the Laplace Eq. (1) and boundary conditions in Eqs. (3)–(6), is linearly proportional to the total charge Q, where Q is related to ΔV from Eq. (2), as to be discussed later.

For the electric potential $\varphi(r,z)$, the Hankel transform of order zero is $\Psi(\xi,z) = \int_0^\infty \varphi(r,z)J_0(\xi r)\,r\,dr$ and its inverse transform is $\varphi(r,z) = \int_0^\infty \Psi(\xi,z)J_0(\xi r)\,\xi\,d\xi$ [17], where J_0 is the 0th-order Bessel function of the first kind. The Hankel transform of Eq. (1) gives:

$$\frac{\partial^2\Psi(\xi,z)}{\partial z^2} - \xi^2\Psi(\xi,z) = 0, \tag{7}$$

which has the solution $\Psi(\xi,z) = A\,e^{-\xi z} + B\,e^{\xi z}$, where A and B are constants to be determined from the boundary conditions. The boundary condition $\partial\varphi/\partial z\big|_{z=h} = 0$ in Eq. (4) gives $A = Be^{2\xi h}$ such that $\Psi(\xi,z) = B\left[e^{\xi(2h-z)} + e^{\xi z}\right]$. The Hankel transform of $-\partial\varphi/\partial z\big|_{z=0}$ in Eqs. (3), (5) and (6) gives $\left[Q/(\pi\varepsilon)\right]\kappa(\xi)$, where:

$$\kappa(\xi) = \frac{J_1(\xi r_c)}{\xi r_c} - \frac{r_{ao}J_1(\xi r_{ao}) - r_{ai}J_1(\xi r_{ai})}{\xi\left(r_{ao}^2 - r_{ai}^2\right)}, \tag{8}$$

and $\int_{x_1}^{x_2} J_0(x)\,x\,dx = x_2J_1(x_2) - x_1J_1(x_1)$ [17] has been used. This gives:

$$B = \frac{Q\kappa(\xi)}{\pi\varepsilon\xi\left(e^{2\xi h} - 1\right)} \tag{9}$$

and

$$\Psi(\xi,z) = \frac{Q}{\pi\varepsilon}\frac{\cosh\left[\xi(h-z)\right]}{\xi\sinh(\xi h)}\kappa(\xi). \tag{10}$$

The electric potential is then obtained from the inverse Hankel transform as:

$$\varphi(r,z) = \frac{Q}{\pi\varepsilon}\int_0^\infty \frac{\cosh\left[\xi(h-z)\right]}{\sinh(\xi h)}J_0(\xi r)\,\kappa(\xi)\,d\xi. \tag{11}$$

It gives the average electric potential over the inner circular and outer annulus electrodes as $2\pi\int_0^{r_c}\varphi\big|_{z=0} r\,dr/\left(\pi r_c^2\right) = 2Q\int_0^\infty J_1(\xi r_c)\,\kappa(\xi)/\left[\xi r_c\tanh(\xi h)\right]\,d\xi/\pi\varepsilon$ and $2\pi\int_{r_{ai}}^{r_{ao}}\varphi\big|_{z=0} r\,dr/\left[\pi\left(r_{ao}^2 - r_{ai}^2\right)\right] = 2Q\int_0^\infty \kappa(\xi)\left[r_{ao}J_1(\xi r_{ao}) - r_{ai}J_1(\xi r_{ai})\right]/\left[\xi\left(r_{ao}^2 - r_{ai}^2\right)\tanh(\xi h)\right]\,d\xi/\pi\varepsilon$, respectively. They replace the electric potentials in Eq. (2) to determine approximately the charge Q in terms of ΔV as:

$$Q\int_0^\infty \frac{\kappa^2(\xi)}{\tanh(\xi h)}d\xi = \frac{\pi\varepsilon}{2}\Delta V. \tag{12}$$

This gives the capacitance $C = Q/\Delta V$ as:

$$C = \frac{\pi\varepsilon}{2\int_0^\infty \kappa^2(\xi)/\tanh(\xi h)\times d\xi}. \tag{13}$$

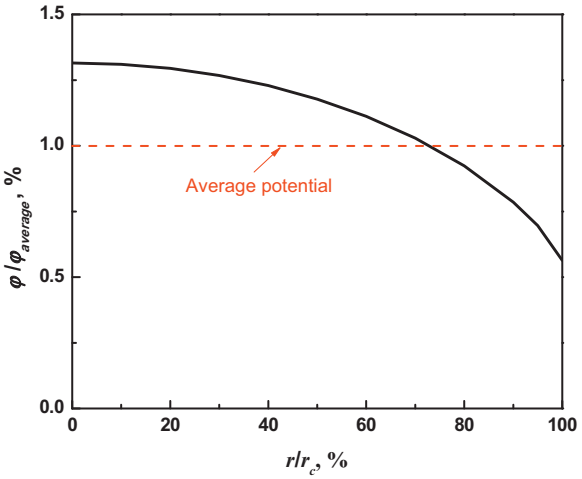

Fig. 2. Comparison of electric potential on inner electrode to the average for r_c = 150 μm, r_{ai} = 200 μm, r_{ao} = 300 μm and h = 1 mm.

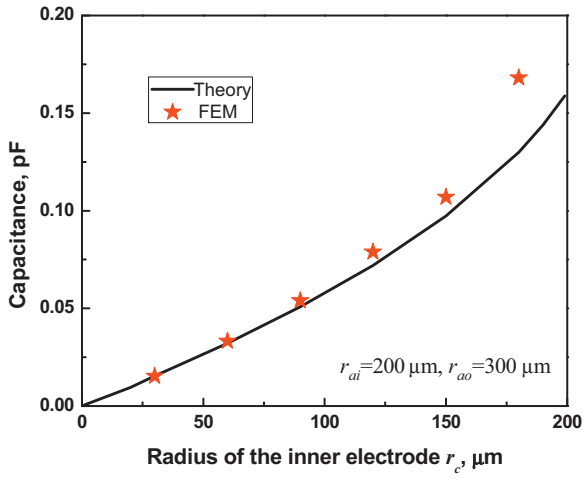

Fig. 3. Capacitance increases as the radius r_c of the inner circular electrode increases (r_{ai} = 200 μm, r_{ao} = 300 μm and $\varepsilon = 15\varepsilon_0$).

The capacitance is linearly proportional to the permittivity of the medium and it also depends on three non-dimensional geometric ratios r_c/r_{ao}, r_{ai}/r_{ao}, h/r_{ao}. It should be noted that Eq. (11) is an approximate solution because Eq. (2) is only satisfied in an averaged sense. As shown in Fig. 2, the electric potential at the inner electrode calculated from Eq. (11) decreases as r increases. This is different from the average, but Eq. (11) is still a very good approximation to calculate capacitance, which is a structural characteristic (instead of a point-wise property) and is in an averaged sense as well.

The capacitance is also calculated by finite element method (FEM) to validate the analytical model. Both stationary heat equation and electrostatics are described by Laplace's equation, where temperature is analogous to electric potential and electric charge can be obtained from heat flux. This thermal-electric analogy enables the calculation of the capacitance from the thermal module in the FEM program ABAQUS [18]. Eight-node quadratic axisymmetric heat transfer quadrilateral elements DCAX8 were used in the ABAQUS finite element program, with very fine mesh near two electrodes. Mesh was refined to ensure the accuracy of numerical results. Both the radius and thickness of the medium are 1 mm, where the electric current density is negligible. The outer radius r_{ao} = 300 μm of the outer annulus electrode and the material parameters are the same as the experiments [10]. Constant boundary condition was assigned to both electrodes, indicating a constant electric potential. Fig. 3 shows that the capacitance increases with the radius r_c of the inner circular electrode, where the inner radius r_{ai} of the outer annulus electrode is fixed at 200 μm. The capacitance decreases as r_{ai} increases, as shown in Fig. 4 for r_c = 150 μm. The numerical results in Figs. 3 and 4 agree well with the analytical results obtained from Eq. (13), particularly for small r_c or relatively large r_{ai}. It needs to be pointed out that the difference between analytical results and measurements becomes larger, when the spacing between inner and outer electrodes gets smaller. This is because the approximation in Eqs. (5) and (6) is not valid for a vanishing spacing, i.e., $r_c \approx r_{ai}$.

In the case of lossy dielectrics, i.e., when the conduction current is not negligible, the permittivity of dielectrics takes a complex form, $\varepsilon = \bar{\varepsilon} - j\sigma/\omega$ [19], where $j = \sqrt{-1}$, $\bar{\varepsilon}$ is the real part of permittivity, ω is angular frequency and σ is the conductivity of dielectrics. Considering the definition of impedance $Z = (j\omega C)^{-1}$ [16], the complex impedance measured by the sensor is derived as:

$$Z = \frac{2}{\pi(\sigma + j\omega\bar{\varepsilon})}\int_0^\infty \frac{\kappa^2(\xi)}{\tanh(\xi h)}\mathrm{d}\xi. \tag{14}$$

The magnitude of the complex impedance measured by the sensor is then obtained analytically as [16]:

$$|Z| = \frac{2}{\pi\sqrt{\sigma^2 + 4\pi^2 f^2 \bar{\varepsilon}^2}}\int_0^\infty \frac{\kappa^2(\xi)}{\tanh(\xi h)}\mathrm{d}\xi, \tag{15}$$

where $f = \omega/(2\pi)$ is the frequency conducted in the measurements.

The real part in Eq. (13) is the effective capacitance C_{eff} of dielectrics and the imaginary part in Eq. (13) contributes to the loss of dielectrics, which is related to the effective resistance R_{eff}. Their relationship $R_{eff} = \bar{\varepsilon}/\left(\sigma C_{eff}\right)$ is consistent with the well-established one for the effective capacitor in parallel with the effective resistor [20].

3. Concentric coplanar capacitor on double-layered media

The skin consists of several layers, but it is common to model them with two layers, stratum corneum (SC) and deep tissue layer (DTL), due to their distinct properties [21]. Fig. 1(c) shows their thickness h_{SC} and h_D. Their electric potentials φ_{SC} and φ_D satisfy Eq. (1).

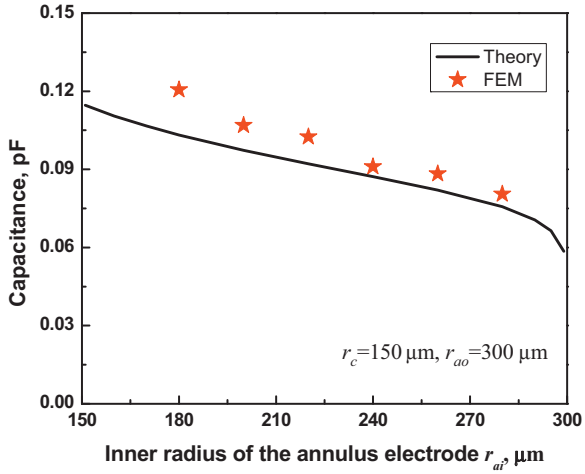

Fig. 4. Capacitance decreases as the inner radius r_{ai} of annulus electrode increases (r_c = 150 μm, r_{ao} = 300 μm and $\varepsilon = 15\varepsilon_0$).

Eqs. (2) and (3) still hold true for SC at $z=0$. Continuity across SC-DTL interface requires:

$$\varphi_{SC}\big|_{z=h_{SC}} = \varphi_D\big|_{z=h_{SC}},\ \varepsilon_{SC}\frac{\partial\varphi_{SC}}{\partial z}\bigg|_{z=h_{SC}} = \varepsilon_D\frac{\partial\varphi_D}{\partial z}\bigg|_{z=h_{SC}}, \tag{16}$$

where ε_{SC} and ε_D are the permittivities of SC and DTL, respectively. Eq. (4) is replaced by:

$$\frac{\partial\varphi_D}{\partial z}\bigg|_{z=h_{SC}+h_D} = 0. \tag{17}$$

The Hankel transform gives the electric potentials in SC and DTL as:

$$\begin{aligned}\varphi_{SC}(r,z) &= \int_0^\infty \left(A_{SC}e^{-\xi z} + B_{SC}e^{\xi z}\right) J_0(\xi r)\,\xi\,d\xi\\ \varphi_D(r,z) &= \int_0^\infty \left(A_D e^{-\xi z} + B_D e^{\xi z}\right) J_0(\xi r)\,\xi\,d\xi.\end{aligned} \tag{18}$$

The boundary conditions from Eqs. (16) and (17) become:

$$\begin{aligned}&A_{SC} - A_D + (B_{SC} - B_D)e^{2\xi h_{SC}} = 0\\ &\varepsilon_{SC}A_{SC} - \varepsilon_D A_D - (\varepsilon_{SC}B_{SC} - \varepsilon_D B_D)e^{2\xi h_{SC}} = 0\\ &A_D = B_D e^{2\xi(h_{SC}+h_D)}.\end{aligned} \tag{19}$$

Similar to the derivation of Eq. (9), the Hankel transform of $-\partial\varphi_{SC}/\partial z\big|_{z=0}$ is $\left[Q/(\pi\varepsilon_{SC})\right]\kappa(\xi)$, which, together with the derivative of Hankel transform of Eq. (18) $-\partial\Psi_{SC}/\partial z\big|_{z=0} = \xi(A_{SC} - B_{SC})$, give the boundary condition at $z=0$ as:

$$A_{SC} - B_{SC} = \frac{Q\kappa(\xi)}{\pi\varepsilon_{SC}\xi}. \tag{20}$$

Eqs. (19) and (20) give A_{SC}, B_{SC}, A_D and B_D as:

$$\begin{Bmatrix}A_{SC}\\ B_{SC}\\ A_D\\ B_D\end{Bmatrix} = \frac{Q\kappa(\xi)}{2\pi\xi}\frac{1}{\varepsilon_D\cosh(\xi h_{SC})\sinh(\xi h_D) + \varepsilon_{SC}\sinh(\xi h_{SC})\cosh(\xi h_D)} * \begin{Bmatrix}\left[\cosh(\xi h_D) + \frac{\varepsilon_D}{\varepsilon_{SC}}\sinh(\xi h_D)\right]e^{\xi h_{SC}}\\ \left[\cosh(\xi h_D) - \frac{\varepsilon_D}{\varepsilon_{SC}}\sinh(\xi h_D)\right]e^{-\xi h_{SC}}\\ e^{\xi(h_{SC}+h_D)}\\ e^{-\xi(h_{SC}+h_D)}\end{Bmatrix}. \tag{21}$$

Similar to the analysis in Section 2, the capacitance C for the double-layered materials is obtained as:

$$C = \frac{\pi\varepsilon_{SC}}{2\int_0^\infty \kappa^2(\xi)\frac{\varepsilon_D\tanh(\xi h_{SC})\tanh(\xi h_D)+\varepsilon_{SC}}{\varepsilon_D\tanh(\xi h_D)+\varepsilon_{SC}\tanh(\xi h_{SC})}\,d\xi}. \tag{22}$$

It degenerates to Eq. (13) when either the thickness h_{SC} or h_D approaches to zero, or when $\varepsilon_D = \varepsilon_{SC}$.

To validate Eq. (22), the capacitance is also calculated by FEM for the radii $r_c = 100\,\mu m$, $r_{ai} = 300\,\mu m$, $r_{ao} = 400\,\mu m$, and thickness $h_{SC} = 20\,\mu m$. The permittivity is $\varepsilon_{SC} = 15\varepsilon_0$ and $\varepsilon_D = 100\varepsilon_0$, where ε_0 is the permittivity in the vacuum. Fig. 5 shows that the capacitance increases with the total thickness (sum of the thicknesses of the SC and DTL), and that the analytical model agrees well with numerical results.

Similar to Eq. (13), the permittivity in Eq. (22) takes complex form as well for lossy dielectric medium, i.e., $\varepsilon_{SC} = \bar{\varepsilon}_{SC} - j\sigma_{SC}/\omega$ and $\varepsilon_D = \bar{\varepsilon}_D - j\sigma_D/\omega$, where $\bar{\varepsilon}_{SC}$ and $\bar{\varepsilon}_D$ are the real parts of permittivity of SC and DTL, σ_{SC} and σ_D are the conductivities of SC and DTL, respectively. The impedance measured by the sensor is derived analytically as:

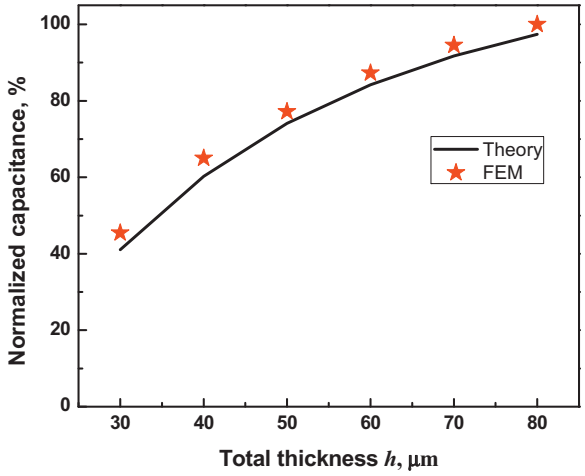

Fig. 5. Capacitance normalized by its maximum value increases as the total thickness (sum of the thicknesses of the stratum corneum and deep tissue layer) increases in the range of [30 μm, 80 μm] ($r_c = 100\,\mu m$, $r_{ai} = 300\,\mu m$, $r_{ao} = 400\,\mu m$, $\varepsilon_{SC} = 15\varepsilon_0$, $\varepsilon_D = 100\varepsilon_0$ and $h_{SC} = 20\,\mu m$ as in experiments).

$$Z = \frac{2}{\pi(\sigma_{SC} + j\omega\bar{\varepsilon}_{SC})}\int_0^\infty \kappa^2(\xi)\frac{(\omega\bar{\varepsilon}_D - j\sigma_D)\tanh(\xi h_{SC})\tanh(\xi h_D) + (\omega\bar{\varepsilon}_{SC} - j\sigma_{SC})}{(\omega\bar{\varepsilon}_D - j\sigma_D)\tanh(\xi h_D) + (\omega\bar{\varepsilon}_{SC} - j\sigma_{SC})\tanh(\xi h_{SC})}\,d\xi. \tag{23}$$

The magnitude of impedance $|Z|$ can then be obtained numerically. For $r_c = 100\,\mu m$, $r_{ai} = 300\,\mu m$, $r_{ao} = 400\,\mu m$, $\varepsilon_{SC} = 15\varepsilon_0$, $\varepsilon_D = 100\varepsilon_0$, $\sigma_{SC} = 10^{-6}$ mS, $\sigma_D = 16$ mS, $h_{SC} = 20\,\mu m$ and $h_D = 30\,\mu m$ as in experiments, a good agreement between Eq. (23) and experimental measurements is shown in Fig. 6. (A detailed description of experiments can be found in [10].) The magnitude of

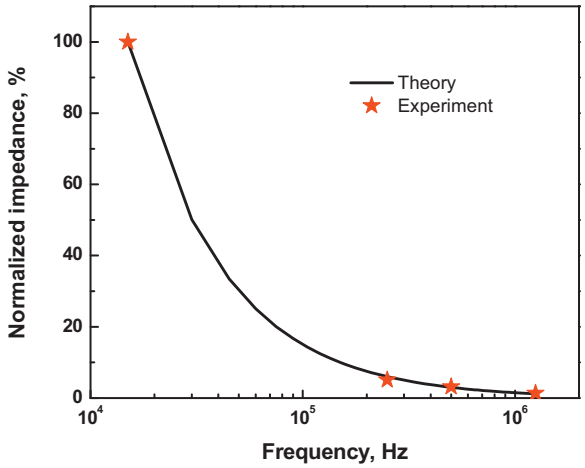

Fig. 6. Capacitance normalized by its maximum value decreases as the frequency increases ($r_c = 100\,\mu m$, $r_{ai} = 300\,\mu m$, $r_{ao} = 400\,\mu m$, $\varepsilon_{SC} = 15\varepsilon_0$, $\varepsilon_D = 100\varepsilon_0$, $\sigma_{SC} = 10^{-6}$ mS, $\sigma_D = 16$ mS, $h_{SC} = 20\,\mu m$ and $h_D = 30\,\mu m$ as in experiments).

impedance decreases as the frequency increases, as observed in the experiments.

4. Concluding remarks

Analytical models of impedance of concentric coplanar capacitors for single- and double-layered structures for epidermal hydration sensing have been established. The expressions quantify the dependence of capacitance/impedance on both the material (conductivity and permittivity) and geometric (radii of inner circular and outer annulus electrodes and thickness of medium layers) parameters. The theoretical predictions calculated from the model agree well with results from FEM and experiments. The model not only offers critical insights into the underlying physics, but also guides parameter optimization in experimental design.

Acknowledgement

Y.H. acknowledges the support from NSF (ECCS-0824129 and CMMI-0749028), and the support from NSFC.

References

[1] K.J. Zhao, M. Pharr, J.J. Vlassak, Z.G. Suo, Inelastic hosts as electrodes for high-capacity lithium-ion batteries, J. Appl. Phys. 109 (1) (2011).
[2] Z.D. Draelos, Cosmetic dermatology: products and procedures, Wiley-Blackwell, 2011.
[3] C. Blichmann, J. Serup, Hydration studies on scaly hand eczema, Contact Dermat. 16 (3) (1987) 155–159.
[4] S.D. Kim, C.H. Huh, K.I. Seo, D.H. Suh, J.I. Youn, Evaluation of skin surface hydration in korean psoriasis patients: a possible factor influencing psoriasis, Clin. Exp. Dermatol. 27 (2) (2002) 147–152.
[5] F.M. Hendriks, D. Brokken, C.W.J. Oomens, F.P.T. Baaijens, Influence of hydration and experimental length scale on the mechanical response of human skin in vivo, using optical coherence tomography, Skin Res. Technol. 10 (4) (2004) 231–241.
[6] D.C. Fowles, R.E. Schneider, Effects of epidermal hydration on skin conductance responses and levels, Biol. Psychol. 2 (1) (1974) 67–77.
[7] E. Uhoda, J.L. Lévêque, G.E. Piérarda, Silicon image sensor technology for in vivo detection of surfactant-induced corneocyte swelling and drying, Dermatology 210 (3) (2005) 184–188.
[8] K. Roth, R. Schulin, H. Fluhler, W. Attinger, Calibration of time domain reflectometry for water-content measurement using a composite dielectric approach, Water Resour. Res. 26 (10) (1990) 2267–2273.
[9] A.A. Anappara, S. Rajeshkumar, P. Mukundan, P.R.S. Warrier, S. Ghosh, K.G.K. Warrier, Impedance spectroscopic studies of sol-gel derived subcritically dried silica aerogels, Acta Mater. 52 (2) (2004) 369–375.
[10] X. Huang, H. Cheng, K. Chen, Y. Zhang, Y. Zhang, Y. Liu, C. Zhu, S.-C. Ouyang, G.-W. Kong, C. Yu, Y. Huang, J.A. Rogers, Epidermal impedance sensing sheets for precision hydration assessment and spatial mapping, IEEE Trans. Biomed. Eng. (2013).
[11] T. Chen, N. Bowler, J.R. Bowler, Analysis of arc-electrode capacitive sensors for characterization of dielectric cylindrical rods, IEEE Trans. Instrum. Meas. 61 (1) (2012) 233–240.
[12] A.A. Nassr, W.H. Ahmed, W.W. El-Dakhakhni, Coplanar capacitance sensors for detecting water intrusion in composite structures, Meas. Sci. Technol. 19 (7) (2008) 075702.
[13] S. Luo, M. Thorburn, V. Tripathi, Modelling of multiple coupled concentric open and closed microstrip ring structure, IEEE Proc. 138 (6) (1991) 573–576.
[14] F. Tefiku, E. Yamashita, Accurate calculation method for the capacitance of generalized circular structures, Int. J. Microwave Mill. 2 (1) (1992) 4–11.
[15] T. Chen, N. Bowler, Analysis of a concentric coplanar capacitive sensor for nondestructive evaluation of multi-layered dielectric structures, IEEE Trans. Dielectr. Electr. Insul. 17 (4) (2010) 1307–1318.
[16] D.J. Griffiths, Reed College, Introduction to Electrodynamics, Prentice Hall, New Jersey, 1999.
[17] R.N. Bracewell, R.N. Bracewell, The Fourier Transform and Its Applications, McGraw-Hill, New York, 1986.
[18] D. Systèmes, Abaqus Analysis User's Manual V6. 9, Dassault Systemes Simulia Corp, Providence, RI, 2009.
[19] J.S. Seybold, Introduction to Rf Propagation www.wiley.com/
[20] J.E. Hall, Access resistance of a small circular pore, J. Gen. Physiol. 66 (4) (1975) 531–532.